

# Soot Nanostructure and Its Impact Upon the O<sub>2</sub> Oxidation Rate

Randy L. Vander Wal, Aaron J. Tomasek  
NCMR c/o NASA-Glenn  
Cleveland, OH 44135

## Introduction

Studies of soot oxidation have ranged from *in situ* flame studies to shock tubes to flow reactors [1]. Each of these systems possesses particular advantages and limitations related to temperature, time and chemical environments. Despite the aforementioned differences, these soot oxidation investigations share three striking features. First and foremost is the wide variation in the rates of oxidation. Reported oxidation rates vary by factors of +6 to - 20 [2] relative to the Nagle Strickland-Constable (NSC) rate for graphite oxidation [3]. Rate variations are not surprising, as the temperatures, residence times, types of oxidants and methods of oxidation differ from study to study. Nevertheless, a valid explanation for rate differences of this magnitude has yet to be presented.

## Experimental

Soots possessing different nanostructures were produced by pyrolysis of acetylene, benzene or ethanol. These soots still in aerosol form were introduced into the post-flame gases produced by a lean, premixed flame supported on a sintered metal burner. A synthetic air mixture consisting of N<sub>2</sub> and O<sub>2</sub> was used for the methane premixed flame. The relative percentages of O<sub>2</sub>/N<sub>2</sub> were varied to maintain the same total “air” flow rate while varying the relative O<sub>2</sub> concentration, thereby maintaining the same “air” heat capacity. To produce an oxidizing gas mixture, all flames used  $\phi < 1$  with a constant methane flow rate of 1.5 slpm. In this manner the adiabatic flame temperature and post-flame gas temperature was maintained nearly constant for this given fuel flow rate. A 5 slpm co-flow of N<sub>2</sub> was used as a shroud.

The soot and a portion of the post combustion gases were directed into a 1 inch outer diameter quartz chimney of 6 inches in length, placed directly above the quartz tube. With this setup, the temperature along the chimney axis was 750 +/- 30 °C, as measured by a type K thermocouple. This variation was within the error range of the thermocouple, +/- 25 °C, and hence it was taken as constant at 750 °C. With a known entrance gas velocity, the residence time of the soot within the chimney is readily calculated based on buoyant acceleration as 75 +/- 5 ms.

Oxidation was conducted well above the flame front, in the post-flame gases. Burning with  $\phi < 1$  ensures that the OH concentration within the post-flame gases is insignificant [10]. Given vastly slower rates for oxidation of carbons by H<sub>2</sub>O or CO<sub>2</sub>, the primary oxidant was considered to be the excess O<sub>2</sub> [1]. The soot stream appeared as a thin cylinder with yellow C<sub>2</sub> Swan band emission associated with burning soot. Partially oxidized soot was collected at the chimney exit by thermophoretic sampling directly upon a lacey TEM grid. A custom image analysis program was scripted for analysis of the HRTEM images using a windows-based, macro interface using Optimus v.6.5.

## Results and Discussion

### Analysis Model

The analysis of the oxidation process is based on a shrinking sphere model, where reactions with oxidizer and corresponding mass loss occur at the particle surface. With this model, changes in the primary particle diameter, as observed using TEM, are readily translated into mass loss per unit surface area. The contribution of internal surface area and pore diffusional effects are

not considered, but this appears justified as detailed in the discussion section for our experimental conditions. It should be noted that this model makes no provisions or assumptions regarding the soot particle structure, active sites, nor mechanism details of the oxidation reactions occurring at the particle surface.

## Results

Figure 1 plots the mass burnout rates versus free O<sub>2</sub> concentration for the soots derived from the different fuels. Burnout rates are calculated relative to the initial particle size before introduction into the flame environment. The mass loss rate increases with increasing O<sub>2</sub> concentration as expected for all soots, yet the soots derived from benzene and acetylene exhibit a dramatic difference in their oxidation rates. As observed, the acetylene soot requires a much higher ambient O<sub>2</sub> concentration to achieve the same level of burnout (for any given reaction duration) as the benzene derived soot. The soot derived from ethanol exhibits a very similar rate as the benzene soot. The faster burnout rate for the benzene and ethanol derived soots is also reflected in their complete oxidation at O<sub>2</sub> concentrations far lower than that of the acetylene derived soot, despite similarly sized primary particles for these two soots. Plotted for reference is the calculated NSC rate at each O<sub>2</sub> concentration at the measured post-flame gas temperature [3]. As seen in Fig. 1, the measured rates for the graphitic acetylene soot lie much closer to the NSC rates. Notably the oxidation rates of all the soots exceed the NSC rate. HRTEM images of the soot have been obtained and reported elsewhere [4]. These images form the basis for our subsequent discussion and lattice fringe analysis as follows next.

## Discussion

### Soot Structure

Although the relation between carbon structure and reactivity is well-known in carbon science from thermal and oxidative studies of coal [5], char [6] and graphite [7]; the relation for soot remains unstudied. It is well-known that graphite oxidation proceeds anisotropically, i.e, the reactivity of basal plane carbon atoms is far lower than that of edge site carbon atoms. Measurements by Rosner and Allendorf observed a 10 - 100-fold reactivity difference between isotropic and pyrolytic graphite, interpreted on the basis of the different reactivities of carbon atoms within basal plane versus edge site positions [7]. Similar variations in the different oxidation rates for natural graphites were observed by Thomas [8] and Henning [9]. Consequently, the observed reactivity will be an average of basal versus edge site carbon atom reactivities for graphitic layer planes of finite dimensions [3]. As the layer plane size decreases, the number of edge site carbon atoms will necessarily increase in proportion to the number of basal plane carbon atoms, allowing one to expect the overall reactivity to increase. In addition to the size of the graphene segments, their relative curvature will also impact their oxidation rate. Curvature arises from 5-membered rings within the aromatic framework [10]. This curvature imposes bond strain because the orbital overlap giving rise to the electronic resonance stabilization is lessened [12]. Therein the C-C bonds are weakened and individual atoms are more exposed, i.e. they are more susceptible to oxidative attack. It is for these same reasons that fullerenes and carbon nanotubes are less resistant towards oxidation than planar graphite [11]. A larger degree of curvature (smaller radius of curvature) increases the imposed bond strain and hence the resistance towards oxidation decreases, as has been found for carbon nanotubes of different diameters [12]. This duality of reactive sites forms the physical basis for the NSC oxidation rate expression which takes into account both edge and basal plane carbon sites and their associated reactivities [3]. However, this semi-empirical rate is based on pyrolytic graphite, a structure with extended basal planes and correspondingly few edge site carbon atoms. Consequently the overall oxidation rate

would be expected to be relatively low compared to most other carbons possessing a less graphitic structure. Notably there is no corresponding model or rate expression that takes into account the curvature of graphitic layer planes and the associated impact upon oxidative stability.

Thus the reactivity of a soot particle towards oxidation depends upon its nanostructure, i.e. the size, orientation and organization of the graphene layer planes. Variations in the graphene layer plane dimensions, curvature, and relative orientation will greatly impact the reactivity of the individual graphene segments, and hence the overall particle reactivity. Yet as discussed, little attention has been given to soot particle nanostructure and its impact upon reactivity towards oxidation within combustion systems. To the degree to which the soot nanostructure reflects a dependence upon inception and growth conditions, so too will its oxidation rate reflect a similar dependence. Our results clearly illustrate a dependence of the burnout rate upon the soot nanostructure as governed here by both the initial fuel and soot growth conditions.

Applying the above discussion to the HRTEM images of our nascent soot samples as have been reported elsewhere [13] and will be presented during the talk, we can compare structural analysis with burnout rates. The benzene derived soot with short, unaligned segments translates into a relatively high percentage of edge site carbon atoms relative to those located at basal plane sites. In contrast, the acetylene derived soot consists of longer graphene segments, which implies a smaller number of edge plane carbon atoms relative to basal plane atoms. Finally, the ethanol derived soot produced similarly long, yet highly curved fringes, which creates high tortuosity, and structural disorder throughout the particle.

### **Lattice Fringe Analysis**

Though the HRTEM images are helpful in revealing the nanostructure of the two soots and provide a basis for interpretation of differences in their oxidation characteristics, alone they provide only a qualitative guide for the measured oxidation rate differences. A more quantitative measure may be obtained by a lattice fringe analysis of the HRTEM images.

Figure 2 plots the histograms of fringe length for each of the three soots. As seen, the fringe length distribution for the acetylene soot extends to much longer graphene layer plane dimensions.

Relative to the distribution for the benzene soot with 80% of the lamella between 0 and 1 nm in length, only 50% of the acetylene fringe length distribution lies between 0 and 1 nm. Alternatively only 2% of the benzene fringe length distribution is greater than 2 nm while 20% of the lamella in the acetylene soot are greater than 2 nm. Of particular interest is that the fringe length histogram for the ethanol derived soot is intermediate between those for the benzene and acetylene derived soots as seen in Fig. 2. (For ethanol, 60% of its fringe length histogram lies between 0 and 1 nm while 13% of the lamella are greater than 2 nm.) Its higher burnout rate clearly points to another factor influencing its reactivity, such as curvature-induced bond strain. The curvature of the graphene segments for the ethanol versus acetylene derived soots is readily apparent upon visual comparison of the the HRTEM images which will be shown. The lattice fringe length distributions serve to quantify the data conveyed by the HRTEM images and provide a firm basis for our conclusions. Future work will be directed towards developing a correlation between the soot nanostructure, as revealed by HRTEM and quantified by fringe analysis, and the soot's oxidation rate.

### **Conclusions**

The work reported here illustrates a dependence of the soot particle nanostructure upon synthesis conditions; namely temperature, time and initial fuel identity. Such structural variations in the graphene layer plane dimensions necessarily alters the ratio of basal plane versus edge site carbon atoms. A corresponding variation in the overall reactivity, reflecting an average of the different reactivities associated with these specific atomic sites arises. This variation is illustrated

here between a disordered soot derived from benzene and a graphitic soot derived from acetylene. Their oxidation rates differ by nearly 5-fold. Curvature of layer planes, as observed for an ethanol derived soot, is found to substantially increase oxidative reactivity. Relative to fringe length as a manifestation of graphitic structure, curvature more effectively increases reactivity towards oxidation. Larger variations in oxidation behavior may be expected, depending upon the soot synthesis conditions. Other physical properties may similarly be affected.

## Acknowledgements

This work was supported by a NASA NRA 99-HEDs-01 combustion award (RVW) administered through NASA cooperative agreement NAC3-975 with The National Center for Microgravity Research on Fluids and Combustion (NCMR) at The NASA-Glenn Research Center. The authors gratefully acknowledge Gordon M. Berger for assistance with the experiments and Dr. Y. L. Chen and David R. Hull for the TEM imaging.

## References

1. Kennedy, I. M., Prog. Energy Combust. Sci. 23:95-132 (1997). (and references therein).
2. Puri, R., Santoro, R. J., and Smyth, K. C., Combust. and Flame 97:125-144 (1994).
3. Nagle, J. Strickland-Constable, R. F., Proc. of the Fifth Carbon Conf. 1, p.154-164 (1962).
4. Vander Wal, R. L., and Tomasek, A. J., Combust. and Flame (in press).
5. Ljubisa, R., Walker, P. L. and Jenkins, R. G., Fuel 62:849 (1983).
6. Davis, K. A., Hurt, R. H., Yang, N. Y. C. and Headley, T. J., Combust. and Flame 100:31-40 (1995).
7. Rosner, D. E. and Allendorf, H. D., AIAA Journal 6:650-654 (1968).
8. Thomas, J. M., Microscopy studies of graphite oxidation, in The Chemistry and Physics of Carbon, (P. L. Walker, Jr., Ed.) Vol. 1, p. 121 (1965).
9. Henning, G. R., Chemistry and Physics of Carbon, (P. L. Walker, Jr., Ed.), Vol. 2 p. 1 (1966).
10. Kroto, H. W., Heath, J. R., O'Brien, S. C., Curl, R. F., and Smalley, R. E., Nature, 318:162-165 (1985).
11. Dresselhaus, M. S., Dresselhaus, G., and Eklund, P. C., Science of Fullerenes and Carbon Nanotubes, Academic Press Inc. (1996).
12. Yang, Y., Zou, H., Wu, B., Li, Q., Zhang, J., Liu, Z., Guo, X., and Du, Z., J. Phys. Chem. B 106:7160-7162 (2002).
13. Vander Wal, R. L., Tomasek, A. J., Street, K. J., and Thompson, W., Environ. Sci. and Technol. (submitted).

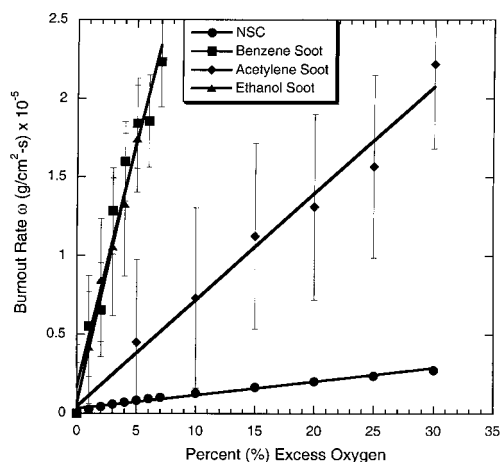


Figure 1 (above). Dependence of soot mass burnout rate with O<sub>2</sub> percentage in the post-flame gases. The NSC rate is also shown for comparison.

Figure 2 (right). Histograms of the lattice fringe lengths for the different indicated soots as obtained by application of the fringe analysis program to the HRTEM images from ref. 4.

